Molecular Crystals and Liquid Crystals

ISSN: 1542-1406 (Print) 1563-5287 (Online) Journal homepage: http://www.tandfonline.com/loi/gmcl20

Computational Study on the Structural and Electronic Properties of Multi-Nuclear Palladium and Nickel Silyl Complexes via DFT and QTAIM Approaches

Tayebeh Hosseinnejad

To cite this article: Tayebeh Hosseinnejad (2014) Computational Study on the Structural and Electronic Properties of Multi-Nuclear Palladium and Nickel Silyl Complexes via DFT and QTAIM Approaches, Molecular Crystals and Liquid Crystals, 605:1, 89-102, DOI: 10.1080/15421406.2014.904995

To link to this article: http://dx.doi.org/10.1080/15421406.2014.904995

Mol. Cryst. Liq. Cryst., Vol. 605: pp. 89–102, 2014

ISSN: 1542-1406 print/1563-5287 online
DOI: 10.1080/15421406.2014.904995

Computational Study on the Structural and Electronic Properties of Multi-Nuclear Palladium and Nickel Silyl Complexes via DFT and QTAIM Approaches

TAYEBEH HOSSEINNEJAD*

Department of Chemistry, Faculty of Science, Alzahra University, Vanak, Tehran, Iran

In this research, we have concentrated on the survey of ability of density functional methods and also modern semi-empirical approaches to reproduce the crystal structure of a binuclear silyl nickel complex and a trinuclear palladium silyl complex. In the structural analysis of the aforesaid nickel and palladium complexes, we have also interested to investigate the possibility of Si-Si bond formation between SiH_2 and μ-SiH moieties from the structural and electronic viewpoints. Comparison of our calculated structural parameters of aforementioned complexes with the available X-ray crystallographical data reveals that both functionals (B3LYP and M062X) can well reproduce X-ray structure of the complex with a near accuracy while the PM6-D2 semi-empirical calculated values are not in a reliable agreement with the crystallographical data. In the next step, we assessed the nature of interactions between palladium and nickel metal ions with silyl ligands via Quantum Theory of Atoms in Molecule (QTAIM) computations. Furthermore, we have analyzed the possibility of Si-Si bond formation in the aforementioned complexes by means of topological electronic indices. Strictly speaking, QTAIM calculations have been performed to explore the electronic density, its laplacian and electronic energy density at some key bond critical points to interpret the structural features of aforesaid complexes from the electronic point of view.

Keywords Binuclear nickel silyl complex; QTAIM approach; semiempirical calculations, DFT method; trinuclear palladium silyl complex

Introduction

Investigation on the structure and reactivity of silyl transition metal complexes is indispensable for the development of new catalytic methodologies. The utility of multinuclear silyl complexes of metals as the versatile catalysis for transformation of organosilicon compounds has been established in many experimental researches [1–3]. Although a number of mononuclear silyl metal complexes are known for all Group10 metals, there are few structurally characterized silylene-bridged multinuclear complexes [4–8].

*Address correspondence to Tayebeh Hosseinnejad. Department of Chemistry, Faculty of Science, Alzahra University, Vanak, Tehran, Iran. Tel.: +98-21-8804-1344; Fax: +98-21-8804-1344. E-mail: tayebeh.hosseinnejad@alzahra.ac.ir

Color versions of one or more of the figures in the article can be found online at www.tandfonline.com/gmcl.

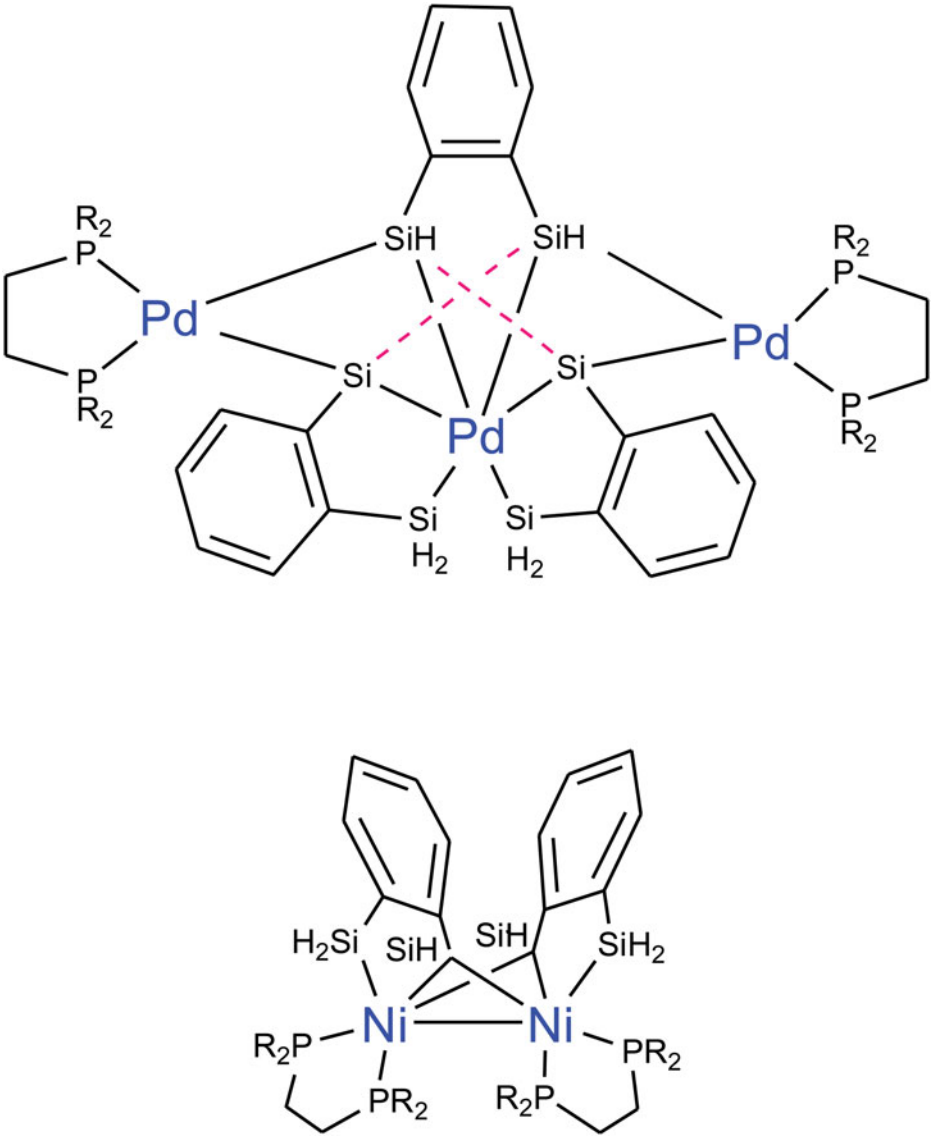

Figure 1. Schematic representation of trinuclear palladium complex with bidentate silyl ligands, **complex-1**, and the dinuclear nickel complex with bidentate silyl ligands, **complex-2**. Note that Si-Si bond formation issue has been illustrated as —- dashed line.

The binuclear (μ-silylene) silyl nickel complexes and also trinuclear palladium complexes with bidentate silyl ligands have been synthesized and surveyed structurally by X-ray crystallography [7,8] (that was illustrated schematically in Fig. 1). The aforementioned trinuclear palladium complex (hereafter denoted as **complex-1**) was synthesized via trimerization reaction of Pd(II) complex bearing the bidentate silyl ligands. Although palladium generally prefers lower oxidation states (Pd ^{0} or Pd ^{II}) and high oxidation states are often attained with highly electronegative ligand, such as fluorides or oxides,

complex-1 was introduced as a formally hexavalent palladium complex with electropositive silyl ligands. In the other hand, the structural analysis of crystallographical data of the aforementioned complex showed that there is short contact between SiH_2 and μ-SiH moieties and consequently Si-Si bond-forming reaction can possibly take place in this complex. So, the central palladium atom is not Pd ^{VI} and the complex can be described as bis σ-complex of Pd ^{II} with Si-Si bonds [9]. This issue has been also surveyed for the dinuclear (μ-silylene) silyl nickel complex (that was illustrated schematically in Fig. 1 and hereafter denoted as **complex-2**) based on X-ray structural data [10].

In this research, we confined our attention on the survey of some structural and electronic aspects of **complex-1** and **complex-2** and the possibility of Si-Si bond formation has been studied using quantum chemistry methods. In the first step, we have examined the ability of density functional theory (DFT) [11,12] and semi-empirical computational methods [13] to predict the crystallographical data of **complex-1** and **complex-2**. In this respect, we have compared the calculated values of structural parameters, obtained via DFT and semi-empirical computations, with the available crystallographical data [9, 10]. The comparison demonstrated a reliable agreement between our obtained optimized geometry with the crystal structure with the preference in using DFT methods in comparison with semi-empirical approach while two DFT methods have the near accuracy in reproducing X-ray structure.

In the next step, since QTAIM approach [14] provides a great deal of information about the nature of bondings, we then assessed the possibility of Si-Si bond formation in **complex-1** and **complex-2** via analysis of the topological properties of electron density, $\rho(r)$, and Laplacian of the electron density,$\nabla^2\rho(r)$, at various bond critical points (BCPs). On the basis of QTAIM electronic energy density indicators, we have characterized quantitatively the covalent or electrostatic natures of metal-ligand interactions in the aforesaid complexes. Furthermore, we have confirmed that Si-Si covalent bond formation could only take place in **complex-1** that is in agreement with the experimental elucidations [9, 10].

Computational Details

Geometry optimization of **complex-1** and **complex-2**, without any symmetry constraint, was performed at semi-empirical PM6-D2 computational level [13] and two levels of DFT methods to assess the performance of these methods in prediction of geometry and energy: (i) 6-31G* using the popular B3LYP level of theory [12] and (ii) 6-31G* basis set with M062X functional which has been introduced recently as a hybrid meta-GGA (generalized gradient approximation) exchange-correlation functional that was parameterized including both transition metals and nonmetals and was recommended for application in organometallic and inorganometallic thermochemistry, kinetic studies, and noncovalent interactions [15, 16]. It is important to state that the popular B3LYP functional is classified as a hybrid functional and incorporate a portion of exact exchange from Hartree-Fock theory with exchange and correlation from ab initio and semi-empirical sources. In general, B3LYP/631G* level of theory is a standard model chemistry with relatively good performance for predicting molecular geometries and vibrational frequencies [17]. Therefore, we have employed M062X as a more modern functional and also as a top performer within 06 modern functionals to compare its performance and accuracy with popular B3LYP functional [18].

It should be noted that although semi-empirical computational methods are not as precise as DFT approach in prediction of molecular structures, but we have employed

PM6-D2 method (which has been recently parameterized to reproduce interaction energies for geometries obtained from high-level quantum mechanical calculations) to evaluate comparatively the ability of this modern semi-empirical method in predicting crystallographical data of **complex-1** and **complex-2.**

In the case of palladium, the effective core potential (ECP), LANL2TZ(f), was used together with the accompanying basis set to describe the valence electron density [19]. All stationary points were characterized as minima after verifying the presence of all real frequencies. All DFT computations have been performed using GAMESS suite of programs [20] and MOPAC 2012 software [21] was utilized for PM6-D2 computations.

Topological analysis of M062X/6-311+G** calculated wave function of electron density at DFT optimized structures of **complex-1** and **complex-2** was performed via QTAIM approach [14, 22]. In this respect, resulting M062X/6-311+G** wave function files were used as inputs to AIM2000 program [23]. Considering the local virial theorem, the following characteristics of BCPs were taken into account: electron density, ρ_b, its Laplacian, $\nabla^2\rho_b$, the electronic kinetic energy density, G_b, the electronic potential energy density, V_b and the total electronic energy density, H_b. These properties have been employed as the useful indicators for quantitative representation of interatomic interactions in the coordination sphere of **complex-1** and **complex-2**.

Result and Discussion

The main objective of this work is to investigate comparatively the ability of computational methods for prediction of X-ray crystal structure of **complex-1** and **complex-2**. In this respect, we have first determined the optimized structure of **complex-1** and **complex-2** using density functional methods and semi-empirical approach. Then a comparison has been made between our calculated bond lengths and angles of **complex-1** and **complex-2**, performed at B3LYP/6-31G* and M062X/6-31G* levels of theory and PM6-D2 method with the available X-ray crystallographical data [9, 10]. It is important to note that the difference between molecular geometries in the gas and solid states arises mainly from the dihedral angles and so, the calculated values of bond lengths and angles in the gas phase are close and so comparable with their corresponded crystallographical data in the solid states.

In Figs. 2 and 3, we have displayed the calculated optimized geometry of **complex-1** and **complex-2** obtained at M062X/6-31G* level, respectively. We have also reported some of selected bond lengths and angles of **complex-1** and **complex-2** calculated at B3LYP/6-31G* and M062X/6-31G* levels of theory and PM6-D2 method, as well as X-ray ones in Tables 1 and 2, respectively. The average absolute deviation (AAD) of X-ray experimental data of **complex-1** with B3LYP/6-31G*, M062X/6-31G*, and PM6-D2 calculated bond lengths are 2.28%, 2.04%, and 4.29%, respectively. Moreover, the AAD of X-ray data of **complex-1** with the calculated bond angles at B3LYP/6-31G*, M062X/6-31G*, and PM6-D2 levels are 3.81%, 3.68%, and 6.32%, respectively. As it can be seen in the reported results of Table 2, the AAD of X-ray experimental data of **complex-2** with B3LYP/6-31G*, M062X/6-31G*, and PM6-D2 calculated bond lengths are 0.97%, 1.11%, and 5.35%, respectively. Moreover, the AAD of X-ray data of **complex-2** with the calculated bond angles at B3LYP/6-31G*, M062X/6-31G*, and PM6-D2 levels are 1.09%, 1.34%, and 6.61%, respectively. Our obtained results indicate that in overall, these computational levels have a reliable agreement with the X-ray structure of complexes while there is a significant superiority in using density functional methods. Furthermore, B3LYP and M062X density functional methods have a near accuracy to reproduce the

Table 1. The selected bond lengths and angles of **complex-1**, calculated at B3LYP/6-31G*, M062X/6-31G*, and PM6-D2 levels of theory together with the X-ray values. Three last columns contain the deviation percents between the calculated results with crystallographical data. Note that numbering of atoms is in accordance with Fig. 2

	Calculated			Experimental X-ray	Dev (%)	
	B3LYP/6-31G*	M062X/6-31G*	PM6-D2	B3LYP/6-31G*	M062X/6-31G*	PM6-D2
Bond lengths (Å)						
Pd(1)-Pd(2)	2.81	2.85	2.98	2.89	−2.76	−1.38	3.11
Pd(1)-Pd(3)	2.95	2.92	2.89	2.91	1.37	0.34	−0.68
Pd(1)-Si(8)	2.37	2.36	2.56	2.34	1.28	0.85	9.40
Pd(1)-Si(9)	2.31	2.32	2.30	2.34	−1.28	−0.85	−1.70
Pd(1)-Si(10)	2.58	2.61	2.54	2.49	3.61	4.81	2.00
Pd(1)-Si(11)	2.40	2.42	2.42	2.44	−1.63	−0.81	−0.81
Pd(1)-Si(12)	2.41	2.42	2.33	2.44	−1.22	−0.81	−4.50
Pd(1)-Si(13)	2.66	2.62	2.68	2.56	3.90	2.34	4.68
Pd(2)-Si(10)	2.40	2.41	2.62	2.37	1.26	1.68	10.54
Pd(2)-Si(12)	2.42	2.38	2.57	2.41	0.41	−1.24	6.63
Pd(3)-Si(11)	2.37	2.36	2.41	2.37	0	−0.42	1.68
Pd(3)-Si(13)	2.35	2.362	2.41	2.39	−1.67	−1.17	0.83
Pd(2)-P(4)	2.39	2.43	2.53	2.32	3.01	4.74	9.05
Pd(2)-P(5)	2.32	2.37	2.45	2.29	1.31	3.49	6.98
Pd(3)-P(6)	2.45	2.44	2.52	2.31	6.06	5.62	9.09
Pd(3)-P(7)	2.43	2.41	2.36	2.29	6.11	5.24	3.05
Si(10)-Si(13)	2.42	2.40	2.43	2.48	−2.41	−3.22	−2.01
Si(11)-Si(12)	2.62	2.68	2.77	2.59	1.15	3.47	6.94
P(4)-C(32)	1.72	1.86	1.95	1.80	−4.44	3.33	8.33
P(5)-C(33)	1.89	1.86	1.95	1.81	4.41	2.76	7.73
P(6)-C(38)	1.89	1.86	1.93	1.84	2.71	1.08	4.89

(Continued on next page)

Table 1. The selected bond lengths and angles of **complex-1**, calculated at B3LYP/6-31G*, M062X/6-31G*, and PM6-D2 levels of theory together with the X-ray values. Three last columns contain the deviation percents between the calculated results with crystallographical data. Note that numbering of atoms is in accordance with Fig. 2 (Continued)

	Calculated			Experimental X-ray	Dev (%)		
	B3LYP/6-31G*	M062X/6-31G*	PM6-D2		B3LYP/6-31G*	M062X/6-31G*	PM6-D2
P(7)-C(39)	1.88	1.85	1.95	1.80	4.44	2.77	8.33
Si(10)-C(19)	1.88	1.89	1.86	1.90	−1.05	−0.52	−2.10
Si(11)-C(25)	1.90	1.89	1.85	1.86	2.15	1.61	−0.53
Si(12)-C(26)	1.90	1.88	1.86	1.87	1.60	0.53	−0.53
Si(13)-C(31)	1.89	1.89	1.86	1.87	1.06	1.06	−0.53
Si(8)-C(14)	1.92	1.91	1.95	1.90	1.05	0.52	2.63
Si(9)-C(20)	1.90	1.90	1.89	1.91	−0.52	−0.52	−1.04
Bond angles (°)							
Pd(2)-Pd(1)-Pd(3)	142.5	141.3	159.4	146.8	−2.92	−3.74	8.58
Pd(2)-Pd(1)-Si(8)	101.0	100.6	109.4	102	−0.98	−1.37	7.25
Pd(2)-Pd(1)-Si(9)	114.7	112.8	121.1	104.2	10.07	8.25	16.21
Pd(2)-Pd(1)-Si(10)	52.9	52.0	53.1	51.6	2.51	0.77	2.90
Pd(2)-Pd(1)-Si(11)	121.9	120.1	110.1	116.5	4.63	3.09	−5.49
Pd(2)-Pd(1)-Si(12)	53.8	53.0	54.7	52.9	1.70	0.18	3.40
Pd(2)-Pd(1)-Si(13)	92.4	93.2	103.3	98.5	−6.19	−5.38	4.87
Pd(3)-Pd(1)-Si(8)	98.0	97.4	88.0	100.8	−2.77	−3.37	−12.6
Pd(3)-Pd(1)-Si(9)	105.5	104.6	107.6	104.8	0.66	−0.19	2.67
Pd(3)-Pd(1)-Si(10)	98.0	96.1	99.8	107.9	−9.17	−10.93	−7.50
Pd(3)-Pd(1)-Si(11)	53.0	51.4	56.5	51.7	2.51	−0.58	9.28
Pd(3)-Pd(1)-Si(12)	105.9	105.7	102.6	103.6	2.22	2.02	−0.96
Pd(3)-Pd(1)-Si(13)	47.9	48.3	46.1	51.3	−6.62	−5.84	−10.13
Si(8)-Pd(1)-Si(9)	75.9	75.1	79.0	74.2	2.29	1.21	6.46

Si(8)-Pd(1)-Si(10)	86.0	85.6	76.9	84	2.38	1.90	−8.45
Si(8)-Pd(1)-Si(11)	139.2	139.1	134.7	139.5	−0.21	−0.28	−3.44
Si(8)-Pd(1)-Si(12)	153.5	153.5	149.2	154.6	−0.71	−0.71	−3.49
Si(8)-Pd(1)-Si(13)	108.9	109.1	114.1	107.8	1.02	1.20	5.84
Si(9)-Pd(1)-Si(10)	152.0	153.2	138.2	143.4	5.99	6.83	−3.62
Si(9)-Pd(1)-Si(11)	87.9	87.1	86.8	84.4	4.14	3.19	2.84
Si(9)-Pd(1)-Si(12)	108.4	110.2	97.1	105.2	3.04	4.75	−7.69
Si(9)-Pd(1)-Si(13)	152.8	152.5	168.7	156.1	−2.11	−2.30	8.07
Si(10)-Pd(1)-Si(11)	119.0	119.3	137.7	129.1	−7.82	−7.59	6.66
Si(10)-Pd(1)-Si(12)	80.5	79.3	90.8	82.3	−2.18	−3.64	10.32
Si(10)-Pd(1)-Si(13)	55.4	55.2	57.1	58.8	−5.78	−6.12	−2.89
Si(11)-Pd(1)-Si(12)	68.4	67.1	58.5	63.95	6.95	4.92	−8.52
Si(11)-Pd(1)-Si(13)	75.9	76.4	85.2	79.2	−4.16	−3.53	7.57
Si(12)-Pd(1)-Si(13)	80.4	78.3	80.9	82.9	−3.01	−5.54	−2.41
Pd(1)-Pd(2)-P(4)	124.4	122.3	122.4	129.6	−4.01	−5.63	−5.55
Pd(1)-Pd(2)-P(5)	124.5	124.3	126.0	129	−3.48	−3.64	−2.32
Pd(1)-Pd(3)-P(6)	119.0	115.9	119.1	125	−4.80	−7.28	−4.72
Pd(1)-Pd(3)-P(7)	118.8	117.4	130.3	124.6	−4.65	−5.77	4.57
Pd(1)-Pd(2)-Si(10)	59.1	58.8	62.4	55.4	6.67	6.13	12.63
Pd(1)-Pd(2)-Si(12)	54.8	54.1	57.5	53.9	1.66	0.37	6.67
Pd(1)-Pd(3)-Si(11)	54.9	53.3	55.9	53.9	1.85	−1.11	3.71
Pd(1)-Pd(3)-Si(13)	59.9	58.7	61.1	56.8	5.45	3.34	7.57

Table 2. The selected bond lengths and angles of **complex-2**, calculated at B3LYP/6-31G*, M062X/6-31G*, and PM6-D2 levels of theory together with the X-ray values. Three last columns contain the deviation percents between the calculated results with crystallographical data. Note that numbering of atoms is in accordance with Fig. 3

	Calculated			Experimental X-ray	Dev (%)		
	B3LYP/6-31G*	M062X/6-31G*	PM6-D2		B3LYP/6-31G*	M062X/6-31G*	PM6-D2
Bond lengths (Å)							
Ni(1)-Ni(2)	2.68	2.62	2.69	2.66	0.75	−1.50	1.12
Ni(1)-Si(7)	2.20	2.19	2.35	2.21	−0.45	−0.90	6.33
Ni(1)-Si(8)	4.23	4.17	4.10	4.19	0.95	−0.47	−2.14
Ni(1)-Si(9)	2.23	2.22	2.38	2.24	−0.44	−0.89	6.25
Ni(1)-Si(10)	2.32	2.35	2.43	2.29	1.31	2.62	6.11
Ni(2)-Si(7)	2.23	2.22	2.33	2.24	−0.44	−0.89	4.01
Ni(2)-Si(8)	2.32	2.35	2.04	2.3	0.86	2.17	−11.30
Ni(2)-Si(9)	2.20	2.19	2.40	2.21	−0.45	−0.90	8.59
Ni(2)-Si(10)	4.23	4.17	4.27	4.2	0.71	−0.71	1.66
Ni(1)-P(3)	2.16	2.16	2.34	2.14	0.93	0.93	9.34
Ni(1)-P(4)	2.20	2.22	2.35	2.18	0.91	1.83	7.79
Ni(2)-P(5)	2.16	2.16	2.32	2.14	0.93	0.93	8.41
Ni(2)-P(6)	2.20	2.22	2.32	2.18	0.91	1.83	6.42
P(3)-C(23)	1.86	1.85	1.94	1.83	1.63	1.09	6.01
P(4)-C(24)	1.87	1.86	1.93	1.84	1.63	1.08	4.89
P(5)-C(29)	1.86	1.85	1.92	1.83	1.63	1.09	4.91
P(6)-C(30)	1.87	1.86	1.96	1.84	1.63	1.08	6.52
Si(7)-Si(10)	2.73	2.63	2.47	2.69	1.48	−2.23	−8.17
Si(8)-Si(9)	2.73	2.63	2.58	2.68	1.86	−1.86	−3.73
Si(7)-C(11)	1.91	1.90	1.86	1.9	0.52	0	−2.10
Si(9)-C(17)	1.91	1.90	1.82	1.9	0.52	0	−4.21
Si(8)-C(16)	1.90	1.89	1.86	1.89	0.52	0	−1.58
Si(10)-C(22)	1.90	1.89	1.85	1.88	1.06	0.53	−1.59
Bond angles (°)							
Ni(1)-Si(7)-Ni(2)	74.3	72.9	66.8	73.4	1.22	−0.68	−8.99
Ni(1)-Si(9)-Ni(2)	74.3	72.9	70.2	73.5	1.08	−0.81	−4.48
Ni(1)-Ni(2)-Si(8)	115.3	113.8	105.9	111	3.87	2.52	−4.59
Ni(2)-Ni(1)-Si(10)	115.3	113.7	107.3	115.4	−0.08	−1.47	−7.01
Si(7)-Ni(1)-Si(9)	83.4	83.3	76.8	83.9	−0.59	−0.71	−8.46
Si(7)-Ni(2)-Si(9)	83.4	83.3	73.9	83.9	−0.59	−0.71	−11.91
Si(7)-Ni(1)-Si(10)	74.4	70.7	76.1	73.3	1.50	−3.54	3.81
Si(9)-Ni(2)-Si(10)	89.5	90.6	84.2	91.4	−2.07	−0.87	−7.87
Si(7)-Ni(2)-Si(8)	90.8	90.6	85.2	91.3	−0.54	−0.76	−6.68
Si(9)-Ni(2)-Si(8)	74.4	70.7	65.6	72.9	2.05	−3.01	−10.01
Ni(1)-Ni(2)-P(5)	128.6	129.6	135.3	129.7	−0.84	−0.07	4.31
Ni(1)-Ni(2)-P(6)	113.7	115.0	103.7	113.9	−0.17	0.96	−8.95
Ni(2)-Ni(1)-P(3)	128.7	129.6	131.9	128.6	0.07	0.77	2.56
Ni(2)-Ni(1)-P(4)	113.7	115.1	116.3	112.9	0.70	1.94	3.01

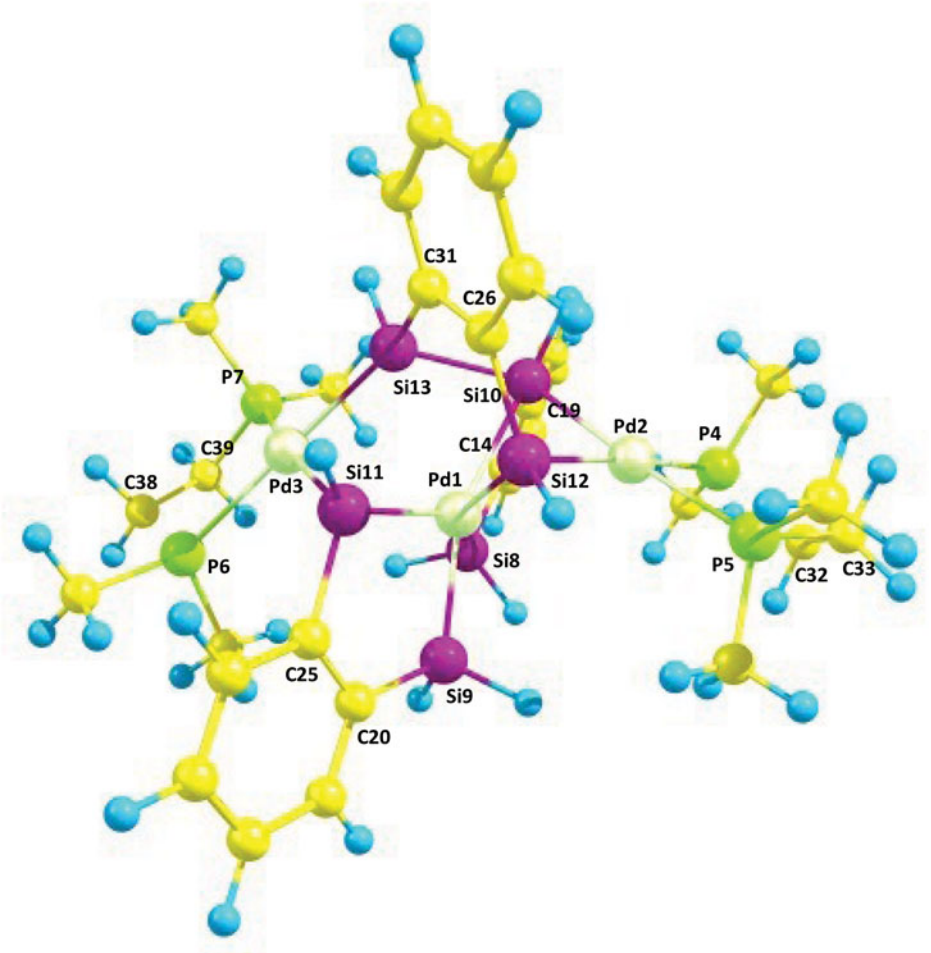

Figure 2. Atomic numbering and energy-minimized structure of **complex-1** obtained at M062X/6-31G* level of theory.

crystallographical data of **complex-1** and **complex-2** [9, 10] and also have predicted the crystal structure of **complex-2** more precisely than **complex-1**.

In the next stage, we concentrated on topological study of electron density to interpret the nature of metal-ligand interactions in **complex-1** and **complex-2**. In this respect, we focused on the QTAIM analysis of M062X/6-311+G** calculated wave function of electron density obtained for the optimized structures of **complex-1** and **complex-2**. Moreover, in order to survey the possibility of Si-Si bond formation, we focused on the calculation of BCPs of M062X/6-311+G** electron density and their associated bond paths on Si10-Si12 and Si11-Si13 in **complex-1** and Si8-Si9 and Si7-Si10 in **complex-2**. QTAIM molecular graph of **complex-1** has been presented in Fig. 4. It should be noticed that due to the large size of **complex-1,** we have not illustrated the whole QTAIM molecular graph. We have shown this molecular graph so that Si-Si bond formation can be illustrated more clearly via bond paths and critical points.

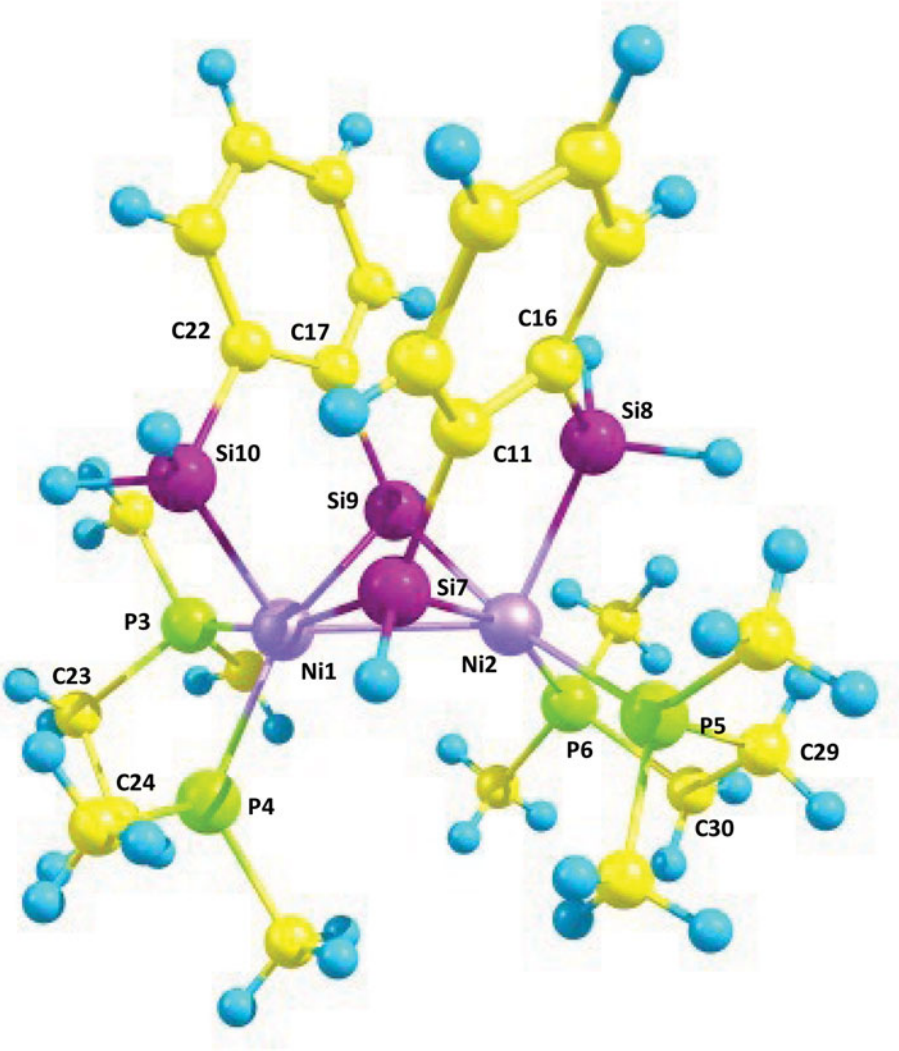

Figure 3. Atomic numbering and optimized structure of **complex-2** obtained at M062X/6-31G* level of theory.

In Tables 3 and 4, we have listed the calculated values of electron density, its laplacian, electronic kinetic energy density, electronic potential energy density, and total electronic energy density of some selected BCPs for **complex-1** and **complex-2,** respectively. It is important to state that the electron density at BCPs usually correlates with the strength of the bond between two atoms. Values of $\rho_b < 0.1$ au are indicative of a closed-shell (i.e., predominantly electrostatic) interaction [22]; it is usually accompanied by a relatively small and positive value of $\nabla^2\rho_b$ [24]. By contrast, for a shared (i.e., predominantly covalent) interaction, ρ_b is usually > 0.1 au [22], and $\nabla^2\rho_b$ is usually negative [25] and typically of the same order as ρ_b. Furthermore, a good reliable indicator for classifying interatomic interactions is the total electronic energy density that is defined as $H_b = G_b + V_b$ at BCPs.

Table 3. Mathematical properties of BCPs associated to Pd-Si and Si-Si interactions in **complex-1**. The properties have been obtained via QTAIM analysis on the M062X/6-311+G** calculated wave function of electron density. Note that numbering of atoms is in accordance with Fig. 2

bonded atoms of BCPs	ρ_b	$\nabla^2\rho_b$	G_b	V_b	H_b	$\lvert V_b\rvert / G_b$
Pd(1)-Si(13)	0.051	0.047	0.026	−0.012	0.014	0.461
Pd(1)-Si(8)	0.084	−0.074	0.028	−0.039	−0.011	1.392
Pd(1)-Si(10)	0.058	0.033	0.028	−0.016	0.012	0.571
Pd(1)-Si(9)	0.082	−0.077	0.028	−0.038	−0.010	1.357
Pd(1)-Si(11)	0.064	0.011	0.029	−0.016	0.013	0.551
Pd(1)-Si(12)	0.065	0.015	0.029	−0.016	0.013	0.551
Pd(2)-Si(10)	0.077	−0.049	0.026	−0.040	−0.014	1.538
Pd(2)-Si(12)	0.075	−0.036	0.025	−0.041	−0.016	1.640
Pd(3)-Si(11)	0.080	−0.053	0.026	−0.038	−0.012	1.461
Pd(3)-Si(13)	0.078	−0.048	0.025	−0.036	−0.011	1.440
Si(10)-Si(12)	0.191	−0.172	0.089	−0.201	−0.112	2.258
Si(11)-Si(13)	0.213	−0.208	0.098	−0.231	−0.133	2.357

In the closed-shell interactions, H_b has the positive value (viz., G_b is dominating) and for shared interactions, it is negative (viz., V_b is dominating).

According to the reported results of Tables 3 and 4, the following facts can be discussed: (i) by considering the positive values of Laplacian of electron density, $\nabla^2\rho_b$, and

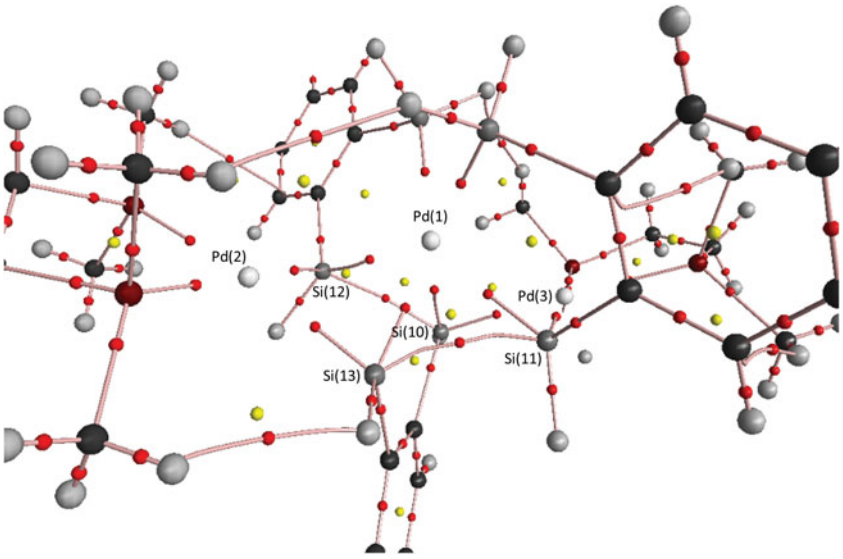

Figure 4. Molecular graph of **complex-1** obtained by QTAIM analysis of M062X/6-311+G** electron density. Bond critical points: red circles; ring critical points: yellow circles; bond paths: pink lines. Note that we have shown this molecular graph so that Si-Si bond formation can be illustrated more clearly.

Table 4. Mathematical properties of BCPs associated to Ni-Si and Si-Si interactions in **complex-2**. The properties have been obtained via QTAIM analysis on the M062X/6-311+G** calculated wave function of electron density. Note that numbering of atoms is in accordance with Fig. 3

bonded atoms of BCPs	ρ_b	$\nabla^2\rho_b$	G_b	V_b	H_b	$\lvert V_b\rvert / G_b$
Ni(1)-Si(9)	0.082	−0.074	0.028	−0.050	−0.022	1.793
Ni(1)-Si(7)	0.085	−0.083	0.030	−0.060	−0.029	1.981
Ni(1)-Si(10)	0.074	−0.023	0.031	−0.048	−0.017	1.546
Ni(2)-Si(7)	0.082	−0.075	0.027	−0.044	−0.016	1.594
Ni(2)-Si(9)	0.085	−0.081	0.030	−0.057	−0.026	1.879
Ni(2)-Si(8)	0.073	−0.018	0.031	−0.055	−0.024	1.784
Si(8)-Si(9)	0.054	0.034	0.012	−0.016	−0.004	1.336
Si(7)-Si(10)	0.053	0.012	0.014	−0.019	−0.005	1.372

its corresponding small values of electron density, ρ_b, at Pd(1)-Si(13), Pd(1)-Si(10), Pd(1)-Si(11), and Pd(1)-Si(12) BCPs in **complex-1**, we can deduce the electrostatic behavior of interactions between Pd-Si. While the negative values of Laplacian of electron density, $\nabla^2\rho_b$, in connection with the larger values of ρ_b at Pd(1)-Si(8), Pd(1)-Si(9), Pd(2)-Si(10), Pd(2)-Si(12), Pd(3)-Si(11), and Pd(3)-Si(13) BCPs in **complex-1** reveal the partially electrostatic and covalent character of Pd-Si interactions. In **complex-2**, we have obtained the negative small calculated values for $\nabla^2\rho_b$ on all Ni-Si BCPs which can be attributed to the semi-covalent semi-electrostatic character of Ni-Si interactions (ii) increasing in the calculated values of ρ_b together with the corresponding $\nabla^2\rho_b$ negative values at Si(10)-Si(12) and Si(11)-Si(13) BCPs in **complex-1** confirms the possibility of Si-Si covalent bond formation which has been elucidated experimentally, while the positive values of $\nabla^2\rho_b$ together with its corresponding small values of ρ_b at Si(8)-Si(9) and Si(7)-Si(10) BCPs of **complex-2** reveals that Si-Si bond formation could not take place in **complex-2**.

Moreover, as it is clear from QTAIM reported results of Tables 3 and 4, the calculated total electronic energy density values at Pd-Si, Ni-Si, and Si-Si BCPs are all in agreement with our earlier interpretations on the nature of interactions. Strictly speaking, the positive values of H_b at Pd(1)-Si(13), Pd(1)-Si(10), Pd(1)-Si(11), and Pd(1)-Si(12) BCPs in **complex-1** correlate with the electrostatic nature of Pd-Si interactions while the small negative values of H_b at Pd(1)-Si(8), Pd(1)-Si(9), Pd(2)-Si(10), Pd(2)-Si(12), Pd(3)-Si(11), and Pd(3)-Si(13) BCPs in **complex-1** and all Ni-Si BCPs in **complex-2** confirms the presence of partially covalent-electrostatic interactions. More importantly, at Si(10)-Si(12) and Si(11)-Si(13) BCPs in **complex-1**, the large negative values of H_b strongly approve the covalent character of Si-Si chemical bonds while the small positive values of H_b at Si(8)-Si(9) and Si(7)-Si(10) BCPs in **complex-2** is in agreement with the impossibility of Si-Si covalent bond forming.

Another reliable indicator for classify interatomic interactions via QTAIM approach has been recently introduced by Espinosa et al. [26] is $\lvert V_b\rvert / G_b$ ratio. On the basis of this suggested indicator, closed-shell interactions are associated with $\lvert V_b\rvert / G_b \leq 1$ (or $H_b = G_b + V_b \geq 0$), intermediate interactions $1 < \lvert V_b\rvert / G_b < 2$, and shared interactions $\lvert V_b\rvert / G_b > 2$. In Tables 3 and 4, we have also summarized the calculated values of $\lvert V_b\rvert / G_b$ ratio for **complex-1** and **complex-2.** Based on the calculated $\lvert V_b\rvert / G_b$ values of **complex-1** and **complex-2,**

we can approve the following facts: (i) electrostatic character of Pd(1)-Si(13), Pd(1)-Si(10), Pd(1)-Si(11), and Pd(1)-Si(12) interactions in **complex-1**, with the corresponding $|V_b|/G_b \leq 1$ values. (ii) Partially covalent-electrostatic nature of Pd(1)-Si(8), Pd(1)-Si(9), Pd(2)-Si(10), Pd(2)-Si(12), Pd(3)-Si(11), and Pd(3)-Si(13) interactions in **complex-1** and all Ni-Si interactions in **complex-2**, with the corresponding $1 < |V_b|/G_b < 2$ values and (iii) the covalent character of Si(10)-Si(12) and Si(11)-Si(13) interactions in **complex-1,** with the corresponding $|V_b|/G_b > 2$ values and semi-covalent semi-electrostatic nature of Si(8)-Si(9) and Si(7)-Si(10) in **complex-2,** with the corresponding $1 < |V_b|/G_b < 2$ values.

Conclusion

As a primary purpose, calculations performed at two levels of DFT (B3LYP/6-31G* and M062X/6-31G*) and PM6-D2 semi-empirical method confirm the following two facts: (i) the ability of DFT methods to reproduce X-ray crystallographical structure of **complex-1** and **complex-2** with a reliable agreement while PM6-D2 semi-empirical approach could not predict accurately the crystal structure of **complex-1** and **complex-2** and (ii) there is a close accuracy between two levels of DFT computations for the prediction of geometry with a relative preference in using M062X functional.

In the next step, the electronic aspects in the crystal structure of **complex-1** and **complex-2** have been studied via topological analysis of electron density and its Laplacian at some selected BCPs. On the basis of several QTAIM electronic energy density indicators, the following facts can be deduced about the nature of metal-ligand interactions: (i) in **complex-1**, the interaction of Pd(1) with Si(10), Si(11), Si(12), and Si(13) has the electrostatic character while other Pd-Si interactions in **complex-1** shows the partially electrostatic and covalent nature, (ii) in **complex-2**, all Ni-Si BCPs demonstrate semi-electrostatic semi-covalent character, and (iii) Si-Si covalent bond formation could only be probable in **complex-1** that is in agreement with the experimental elucidations.

Acknowledgments

The author gratefully acknowledges the partial financial support received from the research council of Alzahra University. The author is also grateful to Prof. M. M. Heravi for his helpful suggestions.

References

[1] Braunstein, P., & Knorr, M. (1995). *J. Organomet. Chem.*, *500*, 21.
[2] Corey, J. Y., & Broddock-Wilking, J. (1999). *Chem. Rev.*, *99*, 175.
[3] Naka, A., Hayashi, M., Okazaki, S., Kunai, A., & Ishikawa, M. (1996). *Organometallics*, *15*, 1101.
[4] Heyn, R. H., & Tilley, T.D. (1992). *J. Am. Chem. Soc.*, *114*, 1917.
[5] Michalczyk, M. J., Recatto, C. A., Calabrese, J. C., & Fink, M. j. (1992). *J. Am. Chem. Soc.*, *114*, 7955.
[6] Suginome, M., Kato, Y., Takeda, N., Oike, H., & Ito, Y. (1998). *Organometallics*, *17*, 495.
[7] Shimada, S., Tanaka, M., & Honda, K. (1995). *J. Am. Chem. Soc.*, *117*, 8289.
[8] Kim, Y. J., Lee, S. C., Park, J. I., Osakada, K., Choi, J. C., & Yamamato, T. (1998). *Organometallics*, *17*, 4929.
[9] Chen, W., Shimada, S., & Tanaka, M. (2002). *Science*, *295*, 308.
[10] Shimada, S., Rao, M. L. N., Hayashi, T., & Tanaka, M. (2001). *Angew. Chem.*, *113*, 219.

[11] Becke, A. D. (1993). *J. Chem. Phys.*, *98*, 1372.
[12] Lee, C., Yang, W., & Parr, R. G. (1988). *Phys. Rev. B*, *37*, 785.
[13] Korth, M., Pitonak, M., Rezac, J., & Hobza, P. A. (2010). *J. Chem. Theory Comput.*, *6*, 344.
[14] Bader, R. F. W. (1990). *Atoms in Molecules: A Quantum Theory*, Oxford University Press: Oxford, UK.
[15] Zhao, Y., Schultz, N. E., & Truhlar, D. G. J. (2006). *Chem. Theory Comput.*, *2*, 364.
[16] Zhao, Y., & Truhlar, D. G. (2008). *Theor. Chem. Acc.*, *120*, 215.
[17] Kruse, H., Goerigk, L., & Grimme, S., (2012). *J. Org. Chem.*, *77*, 10824.
[18] Walker, M., Harvey, A. J. A., Sen, A., & Dessent, C. E. H. (2013). *J. Chem. Phys. A.*, *117*, 12590.
[19] Roy, L. E., Hay, P. J., & Martin, R. L. (2008). *J. Chem. Theory Comput.*, *4*, 1029.
[20] Schmidt, M. W., *et al.* (1993). *J. Comput. Chem.*, *14*, 1347.
[21] MOPAC2012, Stewart, J. J. P. (2012). *Stewart Computational Chemistry, Version 12.157W*, Colorado Springs: USA.
[22] Bader, R. F. W., & Essén, H. (1983). *J. Chem. Phys.*, *80*, 1943.
[23] Bader, R. F. W., (2000). *AIM2000 Program, ver 2.0*, McMaster University: Hamilton.
[24] Bone, R. G. A., & Bader, R. F. W. (1996). *J. Phys. Chem.*, *100*, 10892.
[25] Bobrov, G. V., Popova, G. V., & Tsirelson, V. G. (2006). *Russ. J. Phys. Chem.*, *80*, 584.
[26] Espinosa, E., Alkorta, I., Elguero, J., & Molins, E. (2002). *J. Chem. Phys.*, *117*, 5529.